ACS SENSORS

pubs.acs.org/acssensors

Article

High-Performance Cannabinoid Sensor Empowered by Plant Hormone Receptors and Antifouling Magnetic Nanorods

Zongbo Li, Yuyang Shen, Jesús Beltrán, Hao Tian, Matthew Bedewitz, Ian Wheeldon, Timothy A. Whitehead, Sean R. Cutler, and Wenwan Zhong*

Cite This: *ACS Sens.* 2023, 8, 3914−3922

Read Online

ACCESS | Metrics & More | Article Recommendations | Supporting Information

ABSTRACT: The misuse of cannabinoids and their synthetic variants poses significant threats to public health, necessitating the development of advanced techniques for detection of these compounds in biological or environmental samples. Existing methods face challenges like lengthy sample pretreatment and laborious antifouling steps. Herein, we present a novel sensing platform using magnetic nanorods coated with zwitterionic polymers for the simple, rapid, and sensitive detection of cannabinoids in biofluids. Our technique utilizes the engineered derivatives of the plant hormone receptor *Pyrabactin Resistance 1* (PYR1) as drug recognition elements and employs the chemical-induced dimerization (CID) mechanism for signal development. Additionally, the magnetic nanorods facilitate efficient target capture and reduce the assay duration. Moreover, the zwitterionic polymer coating exhibits excellent antifouling capability, preserving excellent sensor performance in complex biofluids. Our sensors detect cannabinoids in undiluted biofluids like serum, saliva, and urine with a low limit of detection (0.002 pM in saliva and few pM in urine and serum) and dynamic ranges spanning up to 9 orders of magnitude. Moreover, the PYR1 derivatives demonstrate high specificity even in the presence of multiple interfering compounds. This work opens new opportunities for sensor development, showcasing the excellent performance of antifouling magnetic nanorods that can be compatible with different recognition units, including receptors and antibodies, for detecting a variety of targets.

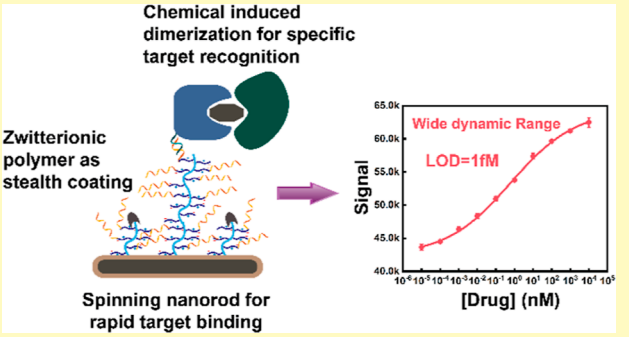

KEYWORDS: *cannabinoids, plant hormone sensors, protein receptors, superparamagnetic nanorods, zwitterionic polymer, ELISA-like assay*

According to the World Drug Report 2022, cannabis is the most widely used controlled drug worldwide.[1] While cannabinoids found in cannabis, like Δ^9-tetrahydrocannabinol (Δ^9-THC) and cannabidiol (CBD), have shown medicinal benefits, including the anti-inflammatory and pain relief properties;[2,3] they also can impair capability of driving, induce negative mental and respiratory health outcomes, and impact the developing brain of adolescents.[4−6] Adding to the concerns is the rising production and use of synthetic cannabinoids (SCs) that can produce strong cannabis-like effects but are marketed as recreational drugs to circumvent legislative control measures.[7] They can induce adverse health effects like seizures, acute respiratory distress syndrome, and multiple organ failure,[8] representing an emerging and ongoing public health and safety threat in the United States.

Timely and proper controls on the abuse of cannabinoids demand the development of specific and sensitive methods for detection of such drugs in biospecimens. The concentration and form of cannabinoids present in biospecimens upon administration are determined by the drug's pharmacokinetics.[9,10] For example, the concentration of intact Δ^9-THC in plasma rapidly decreases after inhalation and can be found at only ∼1 ng/mL or lower in plasma within 24 h.[11,12] Chromatographic separation coupled with multistage mass spectrometry (MS^n) can provide comprehensive analysis and sensitive quantification of the broad spectrum of cannabinoids, achieving limits of detection (LODs) as low as 0.05 ng/mL (∼0.1 nM of common cannabinoids) in well-equipped laboratories.[13,14] Quick exposure assessment in clinical and law-enforcement laboratories at relatively lower costs can be done with enzyme-linked immunosorbent assays (ELISAs) and related immunoassays, reporting LODs ≥ 1−5 ng/mL,[15,16] or activity-based screening assays that offer LODs in the low ng/mL range.[17,18] Electrochemical sensors are more sensitive and can detect as little as 0.0033 ng/mL (10 pM) Δ^9-THC with

Received: July 19, 2023
Accepted: September 8, 2023
Published: September 22, 2023

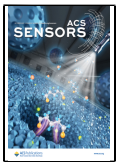

high feasibility for field deployment.[9,19] While these techniques demonstrate good performance, they face two primary challenges: the limited capability to achieve low LOD in unprocessed biological samples without analyte extraction;[13,20,21] and the rapidly emerging SCs that make it difficult to produce the drug recognition units with a matching pace and low cross-reactivity using the conventional ways.[22−24]

To address the need for timely response to the rapidly emerging cannabinoids, we have developed novel phytocannabinoid diagnostic reagents built from engineered plant hormone receptor Pyrabactin Resistance 1 (PYR1). PYR1 recognizes its ligand through the chemically induced dimerization (CID) mechanism, forming a stable PYR1−ligand−protein phosphatase (PP2C) complex.[25] While the CID inhibits the phosphatase activity, the phosphatase acts analogously to a coreceptor to lower the ligand off rates and boost apparent affinity up to ∼100 folds.[26,27] Since the ligand recognition occurs exclusively within PYR1, the engineering of new CID modules can be highly simplified and exploited to design biosensors for diverse chemical classes. In our previous work, we produced several PYR1-derivatives that can selectively recognize various natural and SCs[28] and demonstrated that PYR1-derived receptors can be readily incorporated in ELISA-like assays to achieve sub-nM LODs in serum, saliva, and diluted urine,[28] meeting the needs for detection of cannabinoids and SCs in clinical samples.[29,30]

However, the present ELISA-like assay needs multiple steps as well as several lengthy cycles of surface passivation and washing to remove nonspecific interactions and reduce background, taking more than 1 day to complete. Interference of the matrix components was observed, leading to LODs in complex matrices that were higher than those obtained in the clean saline solution. To speed up detection and enhance assay sensitivity, we employ the superparamagnetic nanorods modified with zwitterionic polymers (**ZIPs**) for rapid detection of the natural and SCs in various biospecimens, including saliva, serum, and urine, within 30 min. Detection of as low as 2.7 fM cannabinoid can be achieved in saliva, and LOD 10−1000 times lower than reported previously is obtained in unprocessed biofluids.[31−37] Our detection platform should have great value for biomedical and clinical analyses of many different types of molecules of interest in addition to the natural and SCs.

EXPERIMENTAL SECTION

Materials and Chemicals. The pooled human serum, saliva, and urine were purchased from Innovative Research. DNA probes used for protein immobilization were synthesized by Integrated DNA Technologies (IDT) [capture probe (**CP**): /5AmMC6/TT TTT TAA CGA CTC ATA TTA ACA A; surface probe (**SP**): /5AmMC6/TT TTT TTG TTA ATA TGA GTC GTT]. Δ^9-THC, cannabidiolic acid (CBDA), CP 47,497, 4F-MDMB, JWH-015, JWH-016, and WIN 55,212-2 were obtained from Cayman Chemical as DEA-exempt preparations where required.

Protein Production. The recombinant PYR1 variants were expressed as 6×-His, 6×-His−maltose binding (MBP), or 6×-His-small ubiquitin-like modifier (SUMO) fusion proteins in *Escherichia coli*, following procedures reported in previous studies[38−40] and described in Supporting Information. They are MBP-PYR1^{WIN}, His-PYR1^{4F}, SUMO-PYR1^{CBDA}, SUMO-PYR1^{THC}, SUMO-PYR1$^{JWH-015}$, SUMO-PYR1$^{JWH-016}$, and SUMO-PYR1^{CP47,497}. All recombinant proteins were purified as described in previously reported studies.[38,40] In brief, sonicated lysates were purified using Ni-NTA agarose (Qiagen) and eluted proteins were dialyzed against 1× Tris-buffered saline (TBS, 20 mM Tris, 150 mM NaCl).

Preparation and Characterization of the Zwitterionic Polymer Layers on the Nanorod Surface. Synthesis of the silica-coated superparamagnetic nanorods (Fe_3O_4@SiO_2 nanorods) followed the reported method;[41] and the steps for nanorod synthesis as well as for coating the nanorods with zwitterionic polymer layers can be found in Supporting Information. The as-prepared nanorods carrying different surface coatings were characterized by multiple techniques. Zeta potential measurements were performed in 1× PBS on a Zetasizer Advance Range (Malvern Analytical) using a folded capillary zeta cell. FT-IR measurements were taken with a Nicolet iS50 FTIR Advanced KBr Gold spectrometer. ^{1}H NMR spectra were recorded by a Bruker Avance NEO 400. Samples for transmission electron microscopy (TEM) were prepared by drying 10 μL of the diluted particle solution on the carbon-coated copper grids and imaged in a Thermo Scientific Talos L120C TEM after drying overnight. The X-ray photoelectron spectroscopy (XPS) was carried out on a Kratos Analytical AXIS Ultra Delay-Line detector (DLD) imaging XPS. Elemental analysis was carried out by an Oxford INCA energy dispersive analytical system (EDS).

Coupling PYR1 and HAB1 Variants with the Capture Probes. The CP modified-PYR1s were prepared *via* click reaction, with details described in Supporting Information, and stored in a solution containing 10% (v/v) glycerol, 50 mM HEPES at pH 8.0, 200 mM KCl, 10 mM $MnCl_2$, 1 mM DTT, and 1 mM TCEP at −80 °C. The conjugates can be stable up to 6 months under this storage condition and were used without purification. They were captured on the surface probe (SP)-conjugated nanorod surface for drug detection *via* hybridization between the CP and SP (Supporting Information).

Ligand/Receptor-Mediated Protein Phosphatase Inhibition Assay. In a typical inhibition assay, the MBP-PYR1^{WIN}-conjugated nanorods were dispersed in 10 μL of the assay buffer (100 mM Tris-HCl, 100 mM NaCl, 30 μg/mL BSA, 1 mM $MnCl_2$, and 0.1% 2-mercaptoethanol). Then, 2 μL of WIN 55,212-2, 5 μL of 2 μM catalytically active His-ΔN-HAB1, 143 μL of the assay buffer, and 40 μL of 5 mM 4-methylumbelliferyl phosphate were mixed and incubated at RT for 10 min on a stirrer. The fluorescence signal was recorded in a Synergy H1 Hybrid Multi-Mode Microplate Reader (BioTek). Alternatively, 5 μL of 2 μM MBP-PYR1^{WIN} was used in the nanorod-free format while keeping other conditions the same.

Nanorod-Assisted ELISA-like Assay. The nanorod-assisted ELISA-like assays were conducted using PYR1 variants and the catalytically inactive, thermo-stabilized MBP-ΔN-HAB1^{T+}.[28] In a typical assay, the PYR1-conjugated nanorods were dispersed in 10 μL of 1× CBSB (a solution containing 20 mM sodium citrate, 147 mM NaCl, 4.5 mM KCl, and 1% BSA) and incubated with 1 μL of the 10 μM biotinylated MBP-ΔN-HAB1^{T+} and 1 μL of the cannabinoid target in different concentrations at RT on a magnetic stirrer for 15 min. After washing the nanorods with 1× CBSB three times, the nanorods were incubated with 10 μL of 0.05 μg/mL streptavidin−HRP prepared in 1× CBSB at RT on the stirrer for another 15 min. Finally, the nanorods were washed with 1× CBSB four times. Signal development was done by adding 100 μL of the SuperSignal West Pico PLUS Chemiluminescent Substrate, and luminescence was read by a BioTek Synergy H1 Hybrid Multi-Mode Microplate Reader.

RESULTS AND DISCUSSION

Design, Fabrication, and Characterization of the ZIP-Coated Nanorods. Slow molecular diffusion to the flat binding surface requires long incubation to ensure target capture, greatly elongating the ELISA-like assays.[28] To speed up target binding, we employed the superparamagnetic Fe_3O_4 nanorods with an average length × width of ∼120 nm × 50 nm to be the solid support for the protein receptors.[41] Besides being easily pulled down by an external magnet, they can rotate on a magnetic stirrer to enhance molecule diffusion, which should greatly speed up ligand capture by PYR1 derivatives and shorten the assay duration. In addition, to enhance the sensitivity of drug detection in biofluids, we fabricated a stealth

https://doi.org/10.1021/acssensors.3c01488
ACS Sens. 2023, 8, 3914−3922

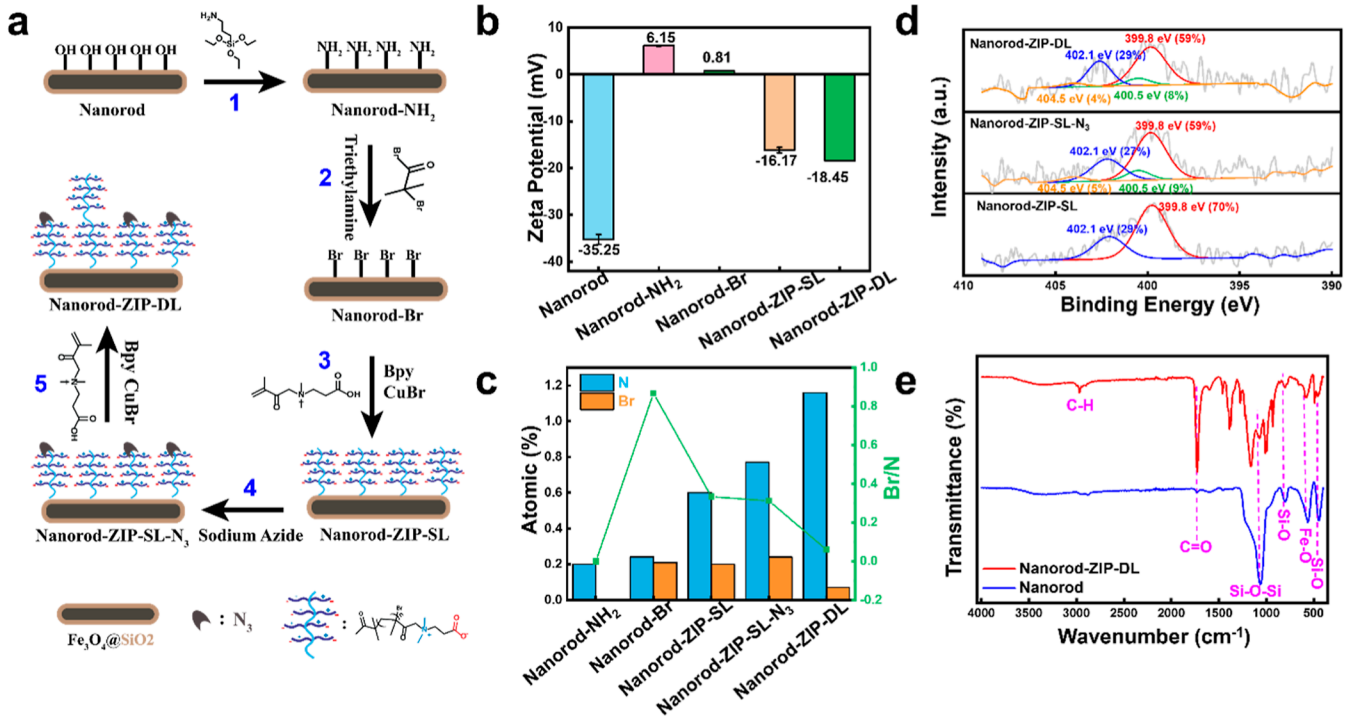

Figure 1. Characterization of the zwitterionic polymer (ZIP) coating on nanorods. (a) The major steps for ZIP production *via* two-step polymerization on nanorods. (b) Zeta potential comparison for the nanorods before polymer coating (nanorod) and after modification with amines (nanorod-NH_2), Br (nanorod-Br), one-step (nanorod-ZIP-SL), and two-step polymerization (nanorod-ZIP-DL), all distributed in the 1× PBS. (c) Elemental analysis and (d) N 1s deconvolution XPS spectra of the nanorod surface obtained after each production step shown in (a). The peaks in (d) at 400.5 and 404.0 eV with a ratio of 2:1 are characteristic of the azide group. (e) FT-IR spectra of the chemical structures found on the nanorod before (blue) and after two-step polymerization (red).

surface by coating the nanorods with the zwitterionic brush polymers of poly(carboxybetaine methacrylate) (poly-CBMA). Zwitterionic polymers can form a stably bounded water layer around the polymer chains to prevent nonspecific protein adsorption.[42] Poly-CBMA also contains rich carboxyl groups that can be used for bioconjugation. Moreover, we attempted a hierarchical polymer growth procedure to have the long and short polymer chains alternatively spaced on the nanorod surface, anticipating that a loosely packed polymer layer could make the conjugation groups more accessible, reduce space hindrance and electrostatic repulsion, and thus enhance the conjugation efficiency.

The major steps of the hierarchical growth of poly-CBMA on the nanorods are illustrated in Figure 1a. In brief, the silica surface of nanorods was first converted to primary amines *via* (3-aminopropyl)triethoxysilane (APTS) treatment (**step 1**) and then reacted with α-bromoisobutylryl bromide to give brominated nanorods (**step 2**), followed by polymerization initiation with the addition of CBMA, CuBr, and 2,2'-bipyridine (bpy) (**step 3**). After 16 h of polymerization, the resultant nanorods referred to as **nanorod-ZIP-single layer (SL)**, the reaction was terminated by addition of sodium azide (**step 4**), which can cap some of the polymer chains by azide and leave others still terminated by Br to support the second round of polymer growth (**step 5**). The product of the two-step polymerization was called the **nanorod-ZIP-dual layer (DL)** to illustrate the presence of long- and short-chain polymers on the nanorod surface.

The changes on the nanorod surface at each synthesis step were characterized carefully. Zeta-potential measurements show that, while amine modification puts positive charges on the initially negatively charged silica surface, substitution of the amine groups by Br neutralized the surface; and growth of the ZIP shifted the surface charges to negative because of its carboxyl groups, with ZIP-DL exhibiting a more negative potential than ZIP-SL because of the addition of more monomers, *i.e.*, more carboxyl groups (Figure 1b).

The atomic percentage (atomic %) of N and Br on the surface of nanorods isolated from each synthesis step was acquired by EDS (Figure 1c). Br was persistently present on the surface after step 2, with little change in its atomic % until a significant drop upon the completion of two-step polymer growth, *i.e.*, step 5. In contrast, the atomic % of N continuously increased in all subsequent steps, illustrating the growth of one polymer layer in step 3, the addition of N_3 in step 4, and the continuous polymer growth in step 5. Agreeing with the reaction design, the ratio of Br/N reached the peak value at step 2, the only step in which the precursor α-bromoisobutylryl bromide was added, and kept decreasing with more and more N bonded to the surface.

Successful azide capping is critical to obtain the hierarchical polymer structure. We carried out XPS to examine the surface chemical composition of the nanorods resulting from steps 3, 4, and 5 (Figures 1d and S2). The N 1s narrow scan (Figure 1d) on nanorod-ZIP-SL exhibited two distinct peaks, representing the bond energy of C−N^+ (402.1 eV) and N−H (399.88 eV) on the monomer. Two additional peaks, 400.5 and 404.0 eV, showed up in the spectra of nanorod-ZIP-SL-N_3 and nanorod-ZIP-DL and have a peak area ratio of 2:1, proving the existence of the azide groups on the nanorod surface after completion of steps 4 and 5.[43,44] These results illustrate the hierarchical polymer growth in steps 3 and 5 from the Br

https://doi.org/10.1021/acssensors.3c01488
ACS Sens. 2023, 8, 3914−3922

reaction center and the presence of N_3 on the surface since step 4 could have prevented further growth of some polymer chains to produce the DL coating.

The final coating produced in **step 5** was examined by FT-IR (Figure 1e). The characteristic band of Fe−O at 569 cm^{-1} was observed, as well as the significant absorption peaks for the asymmetric stretching, symmetric stretching, in-plane bending, and rocking mode of Si−O−Si (1080, 945, 800, and 447 cm^{-1}), proving the integrity of the Fe_3O_4 core and the SiO_2 shell of the nanorods. Several distinct peaks at 1388, 1594, 1724, and 2973 cm^{-1} were observed only on nanorod-ZIP-DL that respectively support the presence of CH_3 (2973 cm^{-1}), C═O (stretching at 1724 cm^{-1}), and COO^- (symmetric stretching at 1388 cm^{-1} and asymmetric stretching at 1594 cm^{-1}) in poly-CBMA. TEM (Figure S1) also confirmed that the polymerization did not alter the uniform core−shell rod structure of the nanorods and maintained their general dimensions to be ∼120 nm long × 25 nm in diameter.

Zwitterionic Feature, Antifouling Capability, and High Conjugation Efficiency of the ZIP. The zwitterionic property of the ZIP was confirmed by zeta-potential measurement (Figure 2a), and the isoelectric point of this polymer coating was found to be at pH 4.4. The ZIP surface would carry net negative charges in biofluids with a pH between 5 and 7.5. The charge-induced repulsion could help the nanorods be well suspended in sample and assay solutions.

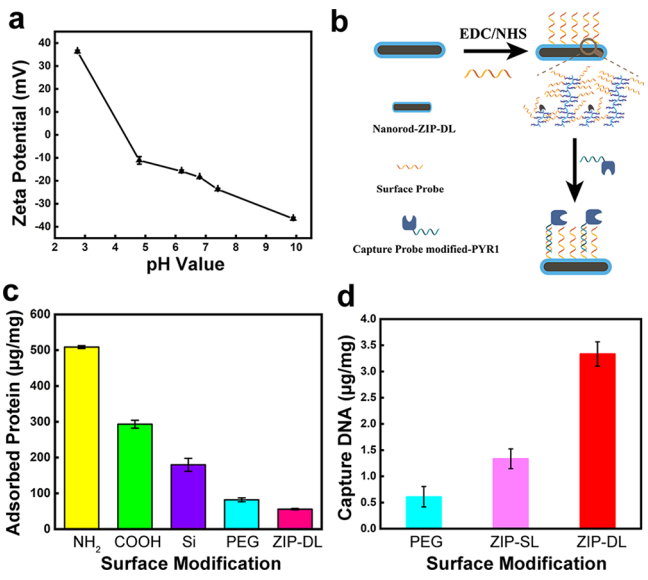

Figure 2. Unique features of the ZIP coating. (a) Zeta potential of nanorod-ZIP-DL measured at different pH values. (b) Comparison of the amount of proteins nonspecifically adsorbed on 1 mg of the nanorods carrying different types of surface coating. (c) Schematic illustration of SP conjugation by EDC/NHS on the ZIP-DL-coated nanorods and immobilization of the capture probe (CP)-conjugated PYR1 through DNA hybridization between the SP and CP. (d) Comparison of the amount of CP immobilized on 1 mg of the nanorods carrying PEG, ZIP-SL, or ZIP-DL as the surface coating.

The antifouling capability of the ZIP was confirmed by evaluating the amounts of proteins adsorbed on the nanorods coated with ZIP-DL, PEG (M_w 350 Da), silica, and silica modified with $-NH_2$ or −COOH when incubated in undiluted human serum. The ZIP-DL surface yielded the lowest amount of protein adsorption, which is ∼30 and 60% lower than that found on the PEG and unmodified silica surface, respectively (Figure 2b), and more than 10× lower than that on the amine- or carboxyl-modified silica surface.

The ZIP contains rich carboxyl groups; and the loosely packed polymer structure obtained from the two-step polymerization should make these functional groups highly accessible for bioconjugation, which would not affect the antifouling property.[45] In our design, the PYR1 proteins are immobilized on the ZIP-coated nanorods for target capture through DNA hybridization (Figure 2c) between the SP conjugated to the nanorods and the CP to the PYR1. The resultant double-stranded DNA (dsDNA) provides sufficient flexibility and rigidity to serve as a cushion between the protein and the solid surface[46] and help maintain the native structure of the conjugated protein.[47,48]

SP immobilization with different amounts of SP inputs with increasing SP input yielded more immobilized SPs on the nanorod-ZIP; but more SPs were conjugated on the nanorod-ZIP-DL, and the SP loadings on the PEG and ZIP-SL surfaces were comparable (Supporting Information Figure S3a,b). These results prove that the two-step polymerization could produce the loosely packed polymer coating for improved accessibility of the functional groups and thus surface conjugation with biomolecules.

We also evaluated the amount of CP captured by the SP-modified nanorods *via* hybridization between the SP and CP. With the conjugation condition that yielded 14 μg of SP per milligram of nanorods, ZIP-DL outperformed ZIP-SL and PEG, capturing the highest amount (3.5 μg) of CP per unit mass of the nanorod (Figure 2d). Since 1 mg of the nanorod contains ∼10^{10} particles, a loading of 3.5 μg of CP per mg of the nanorod means about 28,000 CP molecules were present on each nanorod, and may yield an equivalent amount of PYR1 immobilized on the nanorods. The high number of PYR1 on each nanorod should facilitate rapid drug binding and a high binding capacity. However, increasing SP loading on the nanorods further did not yield more CPs to be captured (Figure S3c), probably because the strong electrostatic repulsion between the negatively charged DNA chains prevented the CP from approaching the nanorod surface for SP hybridization.

Phosphatase Inhibition enhanced by Nanorods for Ultrafast Drug Detection. The phosphatase activity of HAB1 is inhibited upon dimer formation with PYR1 in the presence of drugs. This feature, in conjunction with a fluorogenic phosphatase substrate, can be utilized to design a simple phosphatase inhibition assay for cannabinoid detection. Thus, we tested the performance of such an assay with PYR1 immobilized on the nanorods. Our published work found that MBP-$PYR1^{WIN}$ displayed a half-maximum effective concentration (EC_{50}) value of 72 nM toward (+)-WIN 55,212-2 (henceforth referred to as **WIN**) using the protein phosphatase inhibition assay.[38] We herein chose MBP-$PYR1^{WIN}$ for proof-of-principle studies and conjugated it with the CP for immobilization on the nanorods. Our conjugation condition loaded 3−5 (dibenzocyclooctyne) DBCO molecules per receptor, which should be equivalent to the number of CPs conjugated to each PYR1 (Supporting Information Figure S4).

We found that the activity of His-ΔN-HAB1, the catalytically active HAB1 N-terminal deletion mutant, could be impacted by either physical adsorption or covalent conjugation to the nanorods but not by modification with small molecules like biotin, DBCO, and ssDNA (Supporting Information Figure S5). The inhibitory effect of the nanorods on the

https://doi.org/10.1021/acssensors.3c01488
ACS Sens. 2023, 8, 3914−3922

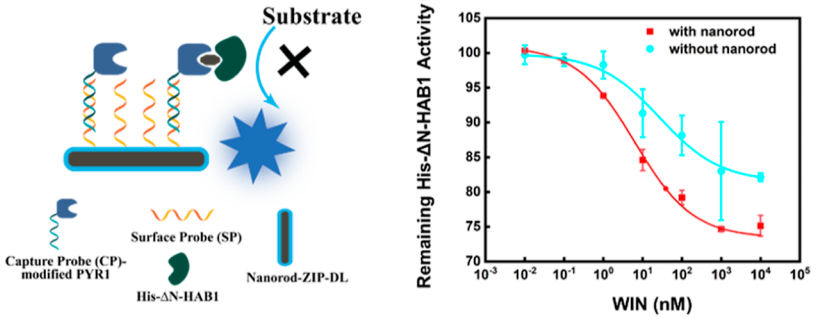

Figure 3. Phosphatase inhibition assay. Titration curves of the ligand-dependent phosphatase inhibition assay performed on the nanorods coated with ZIP-DL (red) or in solution (blue).

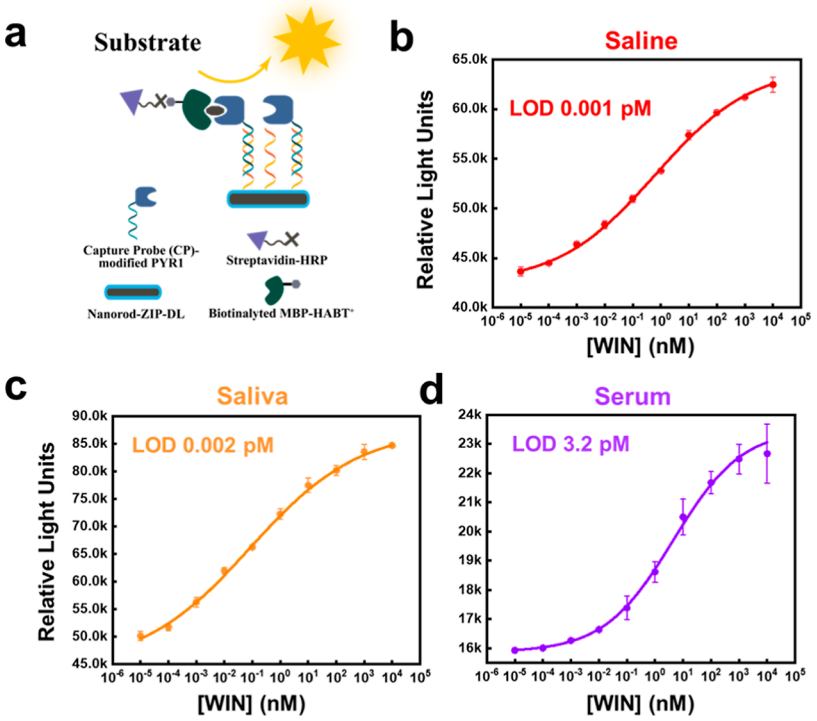

Figure 4. Nanorod-assisted ELISA-like assay. (a) Scheme of the assay: immobilized receptors recruit biotinylated MBP-ΔN-HAB1^{T+} in response to the ligand, and a CL signal is generated by a secondary streptavidin−HRP conjugate. WIN detection in saline (b), undiluted human saliva (c), and serum (d) assisted by nanorod-ZIP-DL. The blank signal in saline, saliva, and serum was 4017 ± 997, 34,700 ± 83, and 12,523 ± 122 light units, respectively. Each data point represents the mean of three replicates, with the error bar representing the standard deviation. The LOD was calculated *via* the 3σ method, equivalent to the drug concentration that would give out a signal equal to 3 times the standard deviation of the blank after blank subtraction.

phosphatase may help enhance signal changes in the phosphatase assay: with the ZIP-DL coating on the nanorods to minimize the nonspecific adsorption of His-ΔN-HAB1, only the specific drug-binding events can bring His-ΔN-HAB1 in close proximity to the nanorods, with its activity reduced by both CID and the nanorods.

Herein, we prepared the MBP-PYR1^{WIN}-conjugated nanorods-ZIP-DL through hybridization between the CP on the MBP-PYR1^{WIN} and the SP on the nanorods to conduct the phosphatase inhibition assay. The resultant nanorods were mixed with 5 μM His-ΔN-HAB1 and WIN at concentrations from 10 pM to 10 μM. The fluorescent signals continuously dropped with increasing WIN concentration, and a faster decrease with the unit increase of the drug concentration was observed with the nanorod-supported assay compared to the in-solution assay (Figure 3), which also yielded an LOD 100× lower. This assay permits ultrafast (taking only 10 min) and simple detection of cannabinoids down to 100 pM for real-world applications because the regulatory guideline of cannabinoids is 3 nM for WIN.[49]

Ultrasensitive Cannabinoid Detection by the Nanorod-Assisted ELISA-like Assay. To achieve even greater sensitivity in cannabinoid detection, we developed the nanorod-assisted ELISA-like assay in which the drug is initially captured by the receptor-conjugated nanorods, and then the biotinylated but catalytically inactive MBP-ΔN-HAB1^{T+} is added to capture the streptavidin−HRP for chemiluminescence (CL) production (Figure 4a).

The calibration curves obtained by using nanorods carrying different surface coatings (PEG, ZIP-SL, and ZIP-DL) for the detection of WIN in saline are shown in Figures 4b and S6. The ZIP surface exhibited significantly higher CL compared to

https://doi.org/10.1021/acssensors.3c01488
ACS Sens. 2023, 8, 3914−3922

PEG, and the signals generated on nanorod-ZIP-DL were ~1.5 times higher than those from ZIP-SL owing to the higher receptor loading enabled by the double-layer ZIP. Remarkably, when compared to assays performed on the conventional multiwell plates, the nanorod-based assays achieved a much lower LOD and a significantly larger dynamic range. In particular, the lowest detectable drug concentration obtained with nanorod-ZIP-DL was 0.01 pM, with the LOD calculated to be 0.001 pM using the 3σ method, and the dynamic range covered over 9 orders of magnitude. This LOD is 10,000× lower and the dynamic range is 6 orders of magnitude wider than the corresponding values reported in our published work that employed the same PYR1/MBP-ΔN-HAB1^{T+} pair in a 96-well plate and the colorimetric substrate of HRP for signal development [the detection results for such an assay using the CL signaling method were worse than absorption detection due to high background and high signal variation (Supporting Information Figure S7)].[28] Such an LOD is also much lower than those in the methods reported so far in the literature for detection of cannabinoids or other controlled drugs (Table S1);[31−37] and our dynamic range is 2−3 orders of magnitude wider than that obtained with the powerful techniques of SIMOA or nanomaterial-based signal amplification for biomarker detection.[50−52]

Furthermore, the antifouling capability of the ZIP enables sensitive drug detection in various complex matrices (Figures 4c,d and S8dd). In contrast to the conventional multiwell plate surface, where detection performance declines substantially in diluted complex matrices, the nanorod-ZIP-DL maintained excellent detection performance in undiluted biofluids. In saliva, the LOD was calculated to be 0.002 pM, comparable to that in saline. Although PEG also demonstrated good antifouling performance (Figure S8a−c), nanorod-ZIP-DL delivered LODs 5−10 times lower, especially in urine and serum, reaching 1.37 pM in urine and 3.2 pM in serum.

The poorer detection performance found in serum and urine than in salvia could be attributed to their different matrix compositions. Serum contains 3−5 mg/mL albumin, which can sequester small molecular drugs and substantially reduce the concentrations of free drugs for PYR1 binding. Urine always exhibits very high background signals when using the PYR1 system for drug detection, probably due to its rich content of metabolites[53] that may compete with cannabinoids for PYR1 binding *via* nonspecific interaction. Normal saliva contains only ~0.5−2 mg/mL total proteins,[54] most of which are salivary proteins with no affinity for drugs; thus, it exhibits the least matrix impact for cannabinoid detection.

Multiplex Detection of Cannabinoids. Our previous work successfully developed 14 PYR1 mutants with specific binding capabilities to various natural and SCs. Thus, we tested in detail the performance of two more receptors, SUMO-PYR1^{THC} and SUMO-PYR1^{CBDA}, in the detection of their corresponding targets, Δ^9-THC and CBDA, on a nanorod platform. We found that Δ^9-THC could be detected with LODs of 0.019 pM in saline and 0.76 pM in saliva, and CBDA detection yielded LODs of 20 pM in saline and 17 pM in saliva, both showing a wide dynamic range extending up to 10 μM (Supporting Information Figure S9). These LODs are not as low as that of WIN, probably due to the lower affinity of these receptors for their target drugs compared to MBP-PYR1^{WIN}. Still, they are more than sufficient for the detection of recent drug exposure.

We further assessed the detection specificity in two ways. First, we compared the CL signal generated by the MBP-PYR1^{WIN}-conjugated nanorod-ZIP-DL when incubated with different drugs at the same concentration. The CL signal generated by the positive target, WIN, was more than 4 times higher than those produced by other drugs (Figure 5a).

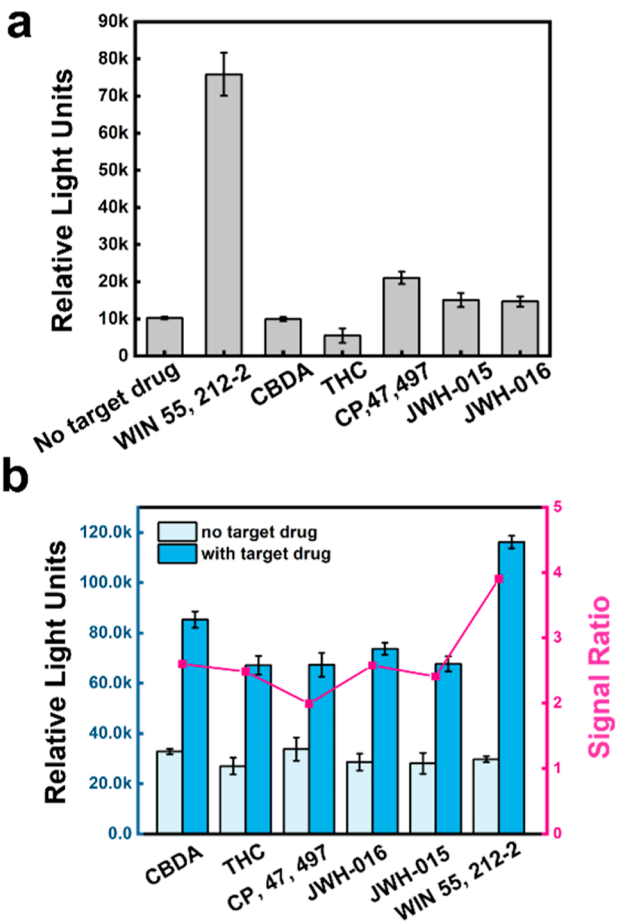

Figure 5. Specificity of the nanorod-assisted ELISA-like assay in cannabinoid detection. (a) Comparison of CL signals produced by 1 μM of WIN, THC, CBDA, JWH-015, JWH-016, CP47, 497, or 4F-MDMB distributed in saline, using the receptor of MBP-PYR1^{WIN}. (b) Bar plots comparing the CL signals generated from the drug mixtures with or without the target drugs, and the curve showing the ratios of the positive (with the target drug) *vs* negative (without the target drug) signals. Each drug in the mixture was at 1 μM. Receptors employed in this experiment were MBP-PYR1^{WIN}, His-PYR1^{4F}, SUMO-PYR1^{CBDA}, SUMO-PYR1^{THC}, SUMO-PYR1$^{JWH-015}$, SUMO-PYR1$^{JWH-016}$, and SUMO-PYR1^{CP47,497}. The results were the average value and the standard deviation (error bar) from three replicates.

Second, we tested the detection of the target drug in the presence of five other drugs using the nanorods conjugated with the corresponding receptor. For example, WIN detection by the MBP-PYR1^{WIN}-conjugated nanorod-ZIP-DL was performed in a solution containing WIN (positive target) and five other drugs (negative targets) mixed at 1 μM each, and the positive signal was compared to that produced by the mixture of the five "negative" targets. All of the receptors tested produced positive signals 2 to 4 times higher than those obtained without the target drug (Figure 5b). One exception was His-PYR1^{4F}, which responded to the negative targets more strongly than to the tested receptors. His-PYR1^{4F} showed little

https://doi.org/10.1021/acssensors.3c01488
ACS Sens. 2023, 8, 3914−3922

cross-reactivity even at high concentrations of WIN when tested in the yeast two-hybrid system or *in vitro* using the ELISA-like assay in multiwell plates and MBP-PYR1^{4F}.[28] However, using the ssDNA-modified His-PYR1^{4F} in our assays, we observe cross-reactivity with WIN, JWH-016, and THC (Supporting Information Figure S10a). This suggests that the tag choice may alter receptor performance and that MBP or SUMO tags are preferable to use over only a 6x-His tag. For the MBP and SUMO-tagged receptors, their signal intensity obtained in our assays is positively correlated with the binding affinity reported previously, indicating a good correlation between sensing performance and receptor-drug binding affinity found in the cell-based screening system (Figure S10b).

CONCLUSIONS

In this study, we fabricated magnetic nanorods coated with a hierarchical double-layer zwitterionic polymer and demonstrated their impressive capability in enhancing the performance of plant hormone receptors for cannabinoid detection. Such a sensor platform can improve molecular diffusion for efficient target capture and fast, as well as sensitive, drug detection. The hierarchical polymer growth produces the loosely packed ZIP layers, delivering high capacity for conjugation of the drug recognition units and minimizing nonspecific protein adsorption for improved signal-to-noise ratios when detecting in undiluted biofluids. Irrespective of the specific method employed, our study showcases the significantly enhanced sensing performance when using the ZIP-coated nanorods as the solid support in immunoassay-like methods. This sensing platform should also be suitable for the employment of a high number of rapidly produced receptors using the high-density mutagenesis PYR1−HAB1 system for the detection of small molecules of interest.

ASSOCIATED CONTENT

Supporting Information

The Supporting Information is available free of charge at https://pubs.acs.org/doi/10.1021/acssensors.3c01488.

Additional method description, nanorod characterization (results from TEM, XPS), ^{1}H NMR of CBDA, primers used in SUMO protein expression and sequences of fusion proteins MBP and SUMO, surface modification comparison (capture efficiency, loading efficiency, and nonspecific adsorption), protein conjugation and its effect on protein activity, and cannabinoid detection performance (PDF)

AUTHOR INFORMATION

Corresponding Author

Wenwan Zhong − *Department of Chemistry and Environmental Toxicology Graduate Program, University of California-Riverside, Riverside, California 92521, United States;* orcid.org/0000-0002-3317-3464; Email: wenwan.zhong@ucr.edu

Authors

Zongbo Li − *Department of Chemistry, University of California-Riverside, Riverside, California 92521, United States*

Yuyang Shen − *Environmental Toxicology Graduate Program, University of California-Riverside, Riverside, California 92521, United States*

Jesús Beltrán − *Department of Botany and Plant Sciences and Institute for Integrative Genome Biology, University of California-Riverside, Riverside, California 92521, United States*

Hao Tian − *Department of Botany and Plant Sciences and Institute for Integrative Genome Biology, University of California-Riverside, Riverside, California 92521, United States*

Matthew Bedewitz − *Department of Chemical and Biological Engineering, University of Colorado Boulder, Boulder, Colorado 80303, United States*

Ian Wheeldon − *Institute for Integrative Genome Biology and Department of Chemical and Environmental Engineering, University of California-Riverside, Riverside, California 92521, United States*

Timothy A. Whitehead − *Department of Chemical and Biological Engineering, University of Colorado Boulder, Boulder, Colorado 80303, United States*

Sean R. Cutler − *Department of Botany and Plant Sciences and Institute for Integrative Genome Biology, University of California-Riverside, Riverside, California 92521, United States*

Complete contact information is available at: https://pubs.acs.org/10.1021/acssensors.3c01488

Notes

The authors declare no competing financial interest.

ACKNOWLEDGMENTS

The research work was supported by the National Institutes of Health/National Institute on Drug Abuse (grant 1R21DA053496-01 to S.R.C. and W.Z.) and the National Science Foundation (NSF-2128287 to T.A.W. and grant NSF-2128016 to S.R.C. and I.W.).

REFERENCES

(1) UNODC, *World Drug Report 2022* (United Nations publication, 2022)

(2) Bhunia, S.; Kolishetti, N.; Arias, A. Y.; Vashist, A.; Nair, M. Cannabidiol for neurodegenerative disorders: a comprehensive review. *Front. Pharmacol* **2022**, *13*, 989717.

(3) Silva-Reis, R.; Silva, A. M. S.; Oliveira, P. A.; Cardoso, S. M. Antitumor Effects of Cannabis sativa Bioactive Compounds on Colorectal Carcinogenesis. *Biomolecules* **2023**, *13*, 764.

(4) Giorgetti, A.; Orazietti, V.; Busardò, F. P.; Giorgetti, R. Psychomotor performances relevant for driving under the combined effect of ethanol and synthetic cannabinoids: A systematic review. *Front. Psychiatry* **2023**, *14*, 1131335.

(5) Scopetti, M.; Morena, D.; Manetti, F.; Santurro, A.; Fazio, N. D.; D'Errico, S.; Padovano, M.; Frati, P.; Fineschi, V. Cannabinoids and Brain Damage: A Systematic Review on a Frequently Overlooked Issue. *Curr. Pharm. Biotechnol.* **2023**, *24*, 741−757.

(6) Hines, L. A.; Freeman, T. P.; Gage, S. H.; Zammit, S.; Hickman, M.; Cannon, M.; Munafo, M.; MacLeod, J.; Heron, J. Association of High-Potency Cannabis Use With Mental Health and Substance Use in Adolescence. *JAMA Psychiatry* **2020**, *77*, 1044−1051.

(7) Tait, R. J.; Caldicott, D.; Mountain, D.; Hill, S. L.; Lenton, S. A systematic review of adverse events arising from the use of synthetic cannabinoids and their associated treatment. *Clin. Toxicol.* **2016**, *54*, 1−13.

(8) Cohen, K.; Weinstein, A. M. Synthetic and Non-synthetic Cannabinoid Drugs and Their Adverse Effects-A Review From Public Health Prospective. *Front. Public Health* **2018**, *6*, 162.
(9) Klimuntowski, M.; Alam, M. M.; Singh, G.; Howlader, M. M. R. Electrochemical Sensing of Cannabinoids in Biofluids: A Noninvasive Tool for Drug Detection. *ACS Sens.* **2020**, *5*, 620−636.
(10) Grotenhermen, F. Pharmacokinetics and Pharmacodynamics of Cannabinoids. *Clin. Pharmacokinet.* **2003**, *42*, 327−360.
(11) Huestis, M. A.; Henningfield, J. E.; Cone, E. J. Absorption of THC and formation of 11-OH-THC and THCCOOH during and after smoking marijuana. *J. Anal. Toxicol.* **1992**, *16*, 276−282.
(12) Gjerde, H.; Beylich, K. M.; Mørland, J. Incidence of alcohol and drugs in fatally injured car drivers in Norway. *Accid. Anal. Prev.* **1993**, *25*, 479−483.
(13) Sim, Y. E.; Kim, J. W.; Ko, B. J.; Kim, J. Y.; Cheong, J. C.; Pyo, J. Determination of urinary metabolites of cannabidiol, Δ8-tetrahydrocannabinol, and Δ9-tetrahydrocannabinol by automated online μSPE-LC-MS/MS method. *J. Chromatogr. B: Anal. Technol. Biomed. Life Sci.* **2023**, *1214*, 123568.
(14) Typek, R.; Holowinski, P.; Dawidowicz, A. L.; Dybowski, M. P.; Rombel, M. Chromatographic analysis of CBD and THC after their acylation with blockade of compound transformation. *Talanta* **2023**, *251*, 123777.
(15) Moody, M. T.; Ringel, M. M.; Mathews, C. M.; Midthun, K. M. Determination of Cross-Reactivity of Contemporary Cannabinoids with THC Direct Immunoassay (ELISA) in Whole Blood. *J. Anal. Toxicol.* **2022**, *46*, 844−851.
(16) Sempio, C.; Wymore, E.; Palmer, C.; Bunik, M.; Henthorn, T. K.; Christians, U.; Klawitter, J. Detection of Cannabinoids by LC−MS-MS and ELISA in Breast Milk. *J. Anal. Toxicol.* **2021**, *45*, 686−692.
(17) Cannaert, A.; Ramirez Fernandez, M. D. M.; Theunissen, E. L.; Ramaekers, J. G.; Wille, S. M. R.; Stove, C. P. Semiquantitative Activity-Based Detection of JWH-018, a Synthetic Cannabinoid Receptor Agonist, in Oral Fluid after Vaping. *Anal. Chem.* **2020**, *92*, 6065−6071.
(18) Cannaert, A.; Storme, J.; Hess, C.; Auwarter, V.; Wille, S. M. R.; Stove, C. P. Activity-Based Detection of Cannabinoids in Serum and Plasma Samples. *Clin. Chem.* **2018**, *64*, 918−926.
(19) Lu, D.; Lu, F.; Pang, G. A Novel Tetrahydrocannabinol Electrochemical Nano Immunosensor Based on Horseradish Peroxidase and Double-Layer Gold Nanoparticles. *Molecules* **2016**, *21* (10), 1377.
(20) Martinez-Perez-Cejuela, H.; Conejero, M.; Amoros, P.; El Haskouri, J.; Simo-Alfonso, E. F.; Herrero-Martinez, J. M.; Armenta, S. Metal-organic frameworks as promising solid-phase sorbents for the isolation of third-generation synthetic cannabinoids in biological samples. *Anal. Chim. Acta* **2023**, *1246*, 340887.
(21) Moorthy, G. S.; Vedar, C.; DiLiberto, M. A.; Zuppa, A. F. A patient-centric liquid chromatography-tandem mass spectrometry microsampling assay for analysis of cannabinoids in human whole blood: Application to pediatric pharmacokinetic study. *J. Chromatogr. B: Anal. Technol. Biomed. Life Sci.* **2019**, *1130−1131*, 121828.
(22) Balaban, S.; Man, E.; Durmus, C.; Bor, G.; Ceylan, A. E.; Pinar Gumus, Z.; Evran, S.; Coskunol, H.; Timur, S. Sensor Platform with a Custom-Tailored Aptamer for Diagnosis of Synthetic Cannabinoids. *Electroanalysis* **2020**, *32*, 656−665.
(23) Yu, H. X.; Luo, Y. P.; Alkhamis, O.; Canoura, J.; Yu, B. Y.; Xiao, Y. Isolation of Natural DNA Aptamers for Challenging Small-Molecule Targets, Cannabinoids. *Anal. Chem.* **2021**, *93*, 3172−3180.
(24) Mascini, M.; Montesano, C.; Perez, G.; Wang, J.; Compagnone, D.; Sergi, M. Selective solid phase extraction of JWH synthetic cannabinoids by using computationally designed peptides. *Talanta* **2017**, *167*, 126−133.
(25) Park, S. Y.; Peterson, F. C.; Mosquna, A.; Yao, J.; Volkman, B. F.; Cutler, S. R. Agrochemical control of plant water use using engineered abscisic acid receptors. *Nature* **2015**, *520*, 545−548.
(26) Ma, Y.; Szostkiewicz, I.; Korte, A.; Moes, D.; Yang, Y.; Christmann, A.; Grill, E. Regulators of PP2C Phosphatase Activity Function as Abscisic Acid Sensors. *Science* **2009**, *324*, 1064−1068.
(27) Szostkiewicz, I.; Richter, K.; Kepka, M.; Demmel, S.; Ma, Y.; Korte, A.; Assaad, F. F.; Christmann, A.; Grill, E. Closely related receptor complexes differ in their ABA selectivity and sensitivity. *Plant J.* **2010**, *61*, 25−35.
(28) Beltran, J.; Steiner, P. J.; Bedewitz, M.; Wei, S.; Peterson, F. C.; Li, Z. B.; Hughes, B. E.; Hartley, Z.; Robertson, N. R.; Medina-Cucurella, A. V.; Baumer, Z. T.; Leonard, A. C.; Park, S. Y.; Volkman, B. F.; Nusinow, D. A.; Zhong, W. W.; Wheeldon, I.; Cutler, S. R.; Whitehead, T. A. Rapid biosensor development using plant hormone receptors as reprogrammable scaffolds. *Nat. Biotechnol.* **2022**, *40*, 1855−1861.
(29) Peterson, B. L.; Couper, F. J. Concentrations of AB-CHMINACA and AB-PINACA and Driving Behavior in Suspected Impaired Driving Cases. *J. Anal. Toxicol.* **2015**, *39*, 642−647.
(30) Hutchison, R. D.; Ford, B. M.; Franks, L. N.; Wilson, C. D.; Yarbrough, A. L.; Fujiwara, R.; Su, M. K.; Fernandez, D.; James, L. P.; Moran, J. H.; Patton, A. L.; Fantegrossi, W. E.; Radominska-Pandya, A.; Prather, P. L. A typical Pharmacodynamic Properties and Metabolic Profile of the Abused Synthetic Cannabinoid AB-PINACA: Potential Contribution to Pronounced Adverse Effects Relative to Δ(9)-THC. *Front. Pharmacol* **2018**, *9*, 1084.
(31) Plouffe, B. D.; Murthy, S. K. Fluorescence-based lateral flow assays for rapid oral fluid roadside detection of cannabis use. *Electrophoresis* **2017**, *38*, 501−506.
(32) Emrani, A. S.; Danesh, N. M.; Ramezani, M.; Taghdisi, S. M.; Abnous, K. A novel fluorescent aptasensor based on hairpin structure of complementary strand of aptamer and nanoparticles as a signal amplification approach for ultrasensitive detection of cocaine. *Biosens. Bioelectron.* **2016**, *79*, 288−293.
(33) Durmus, H.; Durmazel, S.; Uzer, A.; Gokdere, B.; Ercag, E.; Apak, R. Colorimetric Determination of (Aminoalkyl)indole-containing Synthetic Cannabimimetics. *Anal. Sci.* **2018**, *34*, 1419−1425.
(34) Sivashanmugan, K.; Squire, K.; Tan, A. L.; Zhao, Y.; Kraai, J. A.; Rorrer, G. L.; Wang, A. X. Trace Detection of Tetrahydrocannabinol in Body Fluid via Surface-Enhanced Raman Scattering and Principal Component Analysis. *ACS Sens.* **2019**, *4*, 1109−1117.
(35) Xue, W.; Tan, X. T.; Khaing Oo, M. K.; Kulkarni, G.; Ilgen, M. A. A.; Fan, X. D. Rapid and sensitive detection of drugs of abuse in sweat by multiplexed capillary based immuno-biosensors. *Analyst* **2020**, *145*, 1346−1354.
(36) Pholsiri, T.; Lomae, A.; Pungjunun, K.; Vimolmangkang, S.; Siangproh, W.; Chailapakul, O. A chromatographic paper-based electrochemical device to determine Delta(theta)-tetrahydrocannabinol and cannabidiol in cannabis oil. *Sens. Actuators, B* **2022**, *355*, 131353.
(37) Solin, K.; Vuoriluoto, M.; Khakalo, A.; Tammelin, T. Cannabis detection with solid sensors and paper-based immunoassays by conjugating antibodies to nanocellulose. *Carbohydr. Polym.* **2023**, *304*, 120517.
(38) Vaidya, A. S.; Helander, J. D. M.; Peterson, F. C.; Elzinga, D.; Dejonghe, W.; Kaundal, A.; Park, S. Y.; Xing, Z. N.; Mega, R.; Takeuchi, J.; Khanderahoo, B.; Bishay, S.; Volkman, B. F.; Todoroki, Y.; Okamoto, M.; Cutler, S. R. Dynamic control of plant water use using designed ABA receptor agonists. *Science* **2019**, *366*, No. eaaw8848.
(39) Steiner, P. J.; Bedewitz, M. A.; Medina-Cucurella, A. V.; Cutler, S. R.; Whitehead, T. A. A yeast surface display platform for plant hormone receptors: Toward directed evolution of new biosensors. *AIChE J.* **2020**, *66*, No. e16767.
(40) Vaidya, A. S.; Peterson, F. C.; Yarmolinsky, D.; Merilo, E.; Verstraeten, I.; Park, S.-Y.; Elzinga, D.; Kaundal, A.; Helander, J.; Lozano-Juste, J.; Otani, M.; Wu, K.; Jensen, D. R.; Kollist, H.; Volkman, B. F.; Cutler, S. R. A Rationally Designed Agonist Defines Subfamily IIIA Abscisic Acid Receptors As Critical Targets for Manipulating Transpiration. *ACS Chem. Biol.* **2017**, *12*, 2842−2848.

https://doi.org/10.1021/acssensors.3c01488
ACS Sens. 2023, 8, 3914−3922

(41) Li, Z. W.; Jin, J. B.; Yang, F.; Song, N. N.; Yin, Y. D. Coupling magnetic and plasmonic anisotropy in hybrid nanorods for mechanochromic responses. *Nat. Commun.* **2020**, *11*, 2883.
(42) Zhang, Y. X.; Liu, Y. L.; Ren, B. P.; Zhang, D.; Xie, S. W.; Chang, Y.; Yang, J. T.; Wu, J.; Xu, L. J.; Zheng, J. Fundamentals and applications of zwitterionic antifouling polymers. *J. Phys. D Appl. Phys.* **2019**, *52*, 403001.
(43) Lin, Y. M.; Wang, L.; Zhou, J. S.; Ye, L.; Hu, H. Y.; Luo, Z. K.; Zhou, L. Surface modification of PVA hydrogel membranes with carboxybetaine methacrylate via PET-RAFT for anti-fouling. *Polymer* **2019**, *162*, 80−90.
(44) Liu, W. J.; Li, C.; Ren, Y. J.; Sun, X. B.; Pan, W.; Li, Y. H.; Wang, J. P.; Wang, W. J. Carbon dots: surface engineering and applications. *J. Mater. Chem. B* **2016**, *4*, 5772−5788.
(45) Vaisocherova, H.; Yang, W.; Zhang, Z.; Cao, Z. Q.; Cheng, G.; Piliarik, M.; Homola, J.; Jiang, S. Y. Ultralow fouling and functionalizable surface chemistry based on a zwitterionic polymer enabling sensitive and specific protein detection in undiluted blood plasma. *Anal. Chem.* **2008**, *80*, 7894−7901.
(46) Seymour, E.; Daaboul, G. G.; Zhang, X. R.; Scherr, S. M.; Unlu, N. L.; Connor, J. H.; Unlu, M. S. DNA-Directed Antibody Immobilization for Enhanced Detection of Single Viral Pathogens. *Anal. Chem.* **2015**, *87*, 10505−10512.
(47) Leidner, A.; Bauer, J.; Ebrahimi Khonachah, M.; Takamiya, M.; Strahle, U.; Dickmeis, T.; Rabe, K. S.; Niemeyer, C. M. Oriented immobilization of a delicate glucose-sensing protein on silica nanoparticles. *Biomaterials* **2019**, *190−191*, 76−85.
(48) Jia, F.; Narasimhan, B.; Mallapragada, S. Materials-Based Strategies for Multi-Enzyme Immobilization and Co-Localization: A Review. *Biotechnol. Bioeng.* **2014**, *111*, 209−222.
(49) Yu, H.; Lee, H.; Cheong, J.; Woo, S. W.; Oh, J.; Oh, H. K.; Lee, J. H.; Zheng, H.; Castro, C. M.; Yoo, Y. E.; Kim, M. G.; Cheon, J.; Weissleder, R.; Lee, H. A rapid assay provides on-site quantification of tetrahydrocannabinol in oral fluid. *Sci. Transl. Med.* **2021**, *13*, No. eabe2352.
(50) Rissin, D. M.; Fournier, D. R.; Piech, T.; Kan, C. W.; Campbell, T. G.; Song, L. A.; Chang, L.; Rivnak, A. J.; Patel, P. P.; Provuncher, G. K.; Ferrell, E. P.; Howes, S. C.; Pink, B. A.; Minnehan, K. A.; Wilson, D. H.; Duffy, D. C. Simultaneous Detection of Single Molecules and Singulated Ensembles of Molecules Enables Immunoassays with Broad Dynamic Range. *Anal. Chem.* **2011**, *83*, 2279−2285.
(51) Sanjay, S. T.; Li, M. H.; Zhou, W.; Li, X. C.; Li, X. J. A reusable PMMA/paper hybrid plug-and-play microfluidic device for an ultrasensitive immunoassay with a wide dynamic range. *Microsyst. Nanoeng.* **2020**, *6*, 28.
(52) Loynachan, C. N.; Thomas, M. R.; Gray, E. R.; Richards, D. A.; Kim, J.; Miller, B. S.; Brookes, J. C.; Agarwal, S.; Chudasama, V.; McKendry, R. A.; Stevens, M. M. Platinum Nanocatalyst Amplification: Redefining the Gold Standard for Lateral Flow Immunoassays with Ultrabroad Dynamic Range. *ACS Nano* **2018**, *12*, 279−288.
(53) Sarigul, N.; Korkmaz, F.; Kurultak, İ. A New Artificial Urine Protocol to Better Imitate Human Urine. *Sci. Rep.* **2019**, *9*, 20159.
(54) Mohamed, R.; Campbell, J.-L.; Cooper-White, J.; Dimeski, G.; Punyadeera, C. The impact of saliva collection and processing methods on CRP, IgE, and Myoglobin immunoassays. *Clin. Transl. Med.* **2012**, *1*, 19.

https://doi.org/10.1021/acssensors.3c01488
ACS Sens. 2023, 8, 3914−3922